THE JOURNAL OF BIOLOGICAL CHEMISTRY VOL. 290, NO. 2, pp. 1086–1095, January 9, 2015
© 2015 by The American Society for Biochemistry and Molecular Biology, Inc. Published in the U.S.A.

# Organelle-specific Subunit Interactions of the Vertebrate Two-pore Channel Family*

Received for publication, September 8, 2014, and in revised form, November 20, 2014 Published, JBC Papers in Press, December 1, 2014, DOI 10.1074/jbc.M114.610493

**Oluseye A. Ogunbayo[‡1], Yingmin Zhu[§1], Bing Shen[§¶], Ejaife Agbani[‡], Jie Li[¶], Jianjie Ma[‖], Michael X. Zhu[§2], and A. Mark Evans[‡3]**

*From the [‡]Centre for Integrative Physiology, College of Medicine and Veterinary Medicine, University of Edinburgh, Edinburgh EH8 9XD, Scotland, United Kingdom, the [§]Department of Integrative Biology and Pharmacology, The University of Texas Health Science Center at Houston, Houston, Texas 77030, the [¶]Department of Physiology, Anhui Medical University, Hefei, Anhui 230032, China, and the [‖]Department of Surgery, Davis Heart and Lung Research Institute, The Ohio State University Wexner Medical Center, Columbus, Ohio 43210*

**Background:** The role of two-pore channels (TPCs) in endolysosomal signaling remains controversial.
**Results:** TPCs are targeted to different subpopulations of endolysosomes, and this determines subunit interaction and $Ca^{2+}$ signaling by NAADP.
**Conclusion:** All vertebrate TPC subtypes support $Ca^{2+}$ signaling; lysosome-targeted, but not endosome-targeted, TPCs permit endoplasmic reticulum coupling.
**Significance:** Organellar targeting and interaction of TPCs are likely critical to endolysosomal signaling in health and disease.

**The organellar targeting of two-pore channels (TPCs) and their capacity to associate as homo- and heterodimers may be critical to endolysosomal signaling. A more detailed understanding of the functional association of vertebrate TPC1–3 is therefore necessary. We report here that when stably expressed in HEK293 cells, human (h) TPC1 and chicken (c) TPC3 were specifically targeted to different subpopulations of endosomes, hTPC2 was specifically targeted to lysosomes, and rabbit (r) TPC3 was specifically targeted to both endosomes and lysosomes. Intracellular dialysis of NAADP evoked a $Ca^{2+}$ transient in HEK293 cells that stably overexpressed hTPC1, hTPC2, and rTPC3, but not in cells that stably expressed cTPC3. The $Ca^{2+}$ transients induced in cells that overexpressed endosome-targeted hTPC1 were abolished upon depletion of acidic $Ca^{2+}$ stores by bafilomycin $A_1$, but remained unaffected following depletion of endoplasmic reticulum stores by thapsigargin. In contrast, $Ca^{2+}$ transients induced via lysosome-targeted hTPC2 and endolysosome-targeted rTPC3 were abolished by bafilomycin $A_1$ and markedly attenuated by thapsigargin. NAADP induced marked $Ca^{2+}$ transients in HEK293 cells that stably coexpressed hTPC2 with hTPC1 or cTPC3, but failed to evoke any such response in cells that coexpressed interacting hTPC2 and rTPC3 subunits. We therefore conclude that 1) all three TPC subtypes may support $Ca^{2+}$ signaling from their designate acidic stores, and 2) lysosome-targeted (but not endosome-targeted) TPCs support coupling to the endoplasmic reticulum.**

Two-pore segment channel genes (*TPCN1–3*) are present in most vertebrate species, with the complete absence of *TPCN3* in primates (including humans) and some rodents (*e.g.* mice and rats) (1). These genes encode the two-pore channel family (TPC1–3),[4] of which TPC1 was first cloned in 2000 (2). Until recently, however, no functional activity had been determined, and the subcellular distribution of TPCs had not been defined until our proposal that TPC1–3 represent a novel family of endolysosome-targeted channels (1, 3). The majority of our findings have since been confirmed by others (4–8). However, the role of TPCs in endolysosomal $Ca^{2+}$ signaling remains controversial on the grounds of ion selectivity and the capacity for TPC gating by the $Ca^{2+}$-mobilizing messenger NAADP (9–13).

That aside, our initial study also suggested that when stably overexpressed in HEK293 cells, human (h) TPC1 is specifically targeted to endosomes, hTPC2 is specifically targeted to lysosomes, and chicken (c) TPC3 is specifically targeted to recycling endosomes and other as yet unidentified organelles (1, 3). That there are multiple TPCs and that each may be targeted to different intracellular organelles imply that each TPC subtype may underpin spatially segregated and thus compartmentalized signaling via endosomes and lysosomes, respectively. That this may be the case is also open to question, given that more widespread distribution of hTPC1 (6) and sea urchin TPC1 (4) across endosomes, lysosomes, and even the endoplasmic reticulum (ER) has been reported. Then again, such promiscuity could increase the complexity of signal modulation through, for example, the formation of homo- and heterodimers by TPC1 and TPC2 interaction on the same membrane. This possibility of complex subunit interactions was further highlighted by the proposal that sea urchin TPC3 may be dominant-negative for

* This work was supported by National Institutes of Health Grant R01 GM092759 (to M. X. Z.) and by British Heart Foundation Project and Programme Grants PG/10/95/28657 and RG/12/14/29885 (to A. M. E.).
[1] Both authors contributed equally to this work.
[2] To whom correspondence may be addressed. Fax: 713-500-7444; E-mail: michael.x.zhu@uth.tmc.edu.
[3] To whom correspondence may be addressed. Fax: 44-131-650-6527; E-mail: mark.evans@ed.ac.uk.

[4] The abbreviations used are: TPC, two-pore channel; hTPC, human TPC; cTPC, chicken TPC; rTPC, rabbit TPC; ER, endoplasmic reticulum; PNGase F, peptide:*N*-glycosidase F; CICR, $Ca^{2+}$-induced $Ca^{2+}$ release; co-IP, co-immunoprecipitation.

other sea urchin TPCs (4, 8), although other studies have suggested that sea urchin TPC3 supports $Ca^{2+}$ signals (8). That said, there is limited sequence homology with any vertebrate TPC3 (1, 14), and curiously, therefore, zebrafish TPC3 has recently been proposed to act as a plasma membrane-resident, non-inactivating, high voltage-activated sodium channel (15).

In this study, we sought to resolve the aforementioned controversies. Our findings suggest that all three TPC subtypes permit $Ca^{2+}$ signaling in response to NAADP. Only lysosome-targeted hTPC2 and rabbit (r) TPC3 support functional coupling of lysosomal $Ca^{2+}$ release to ER $Ca^{2+}$ mobilization. Curiously, however, although rTPC3, which is targeted to endosomes and lysosomes, appears to form inactive complexes with hTPC2, we found no evidence to support the view that vertebrate TPC3 represents a dominant-negative subtype.

## EXPERIMENTAL PROCEDURES

*Expression Vectors and Cell Culture*—cDNAs for hTPC1, hTPC2, rTPC3, and cTPC3 were fused with mCherry at the N termini and placed in a modified vector in which the cDNA of interest is driven by the human cytomegalovirus promoter and is followed by an internal ribosome entry site sequence added before the coding sequence of the *Streptoalloteichus hindustanus ble* gene, which confers resistance to Zeocin (Invitrogen). cDNAs for hTPC1, hTPC2, rTPC3, cTPC3, and the human transferrin receptor were also placed in pEGFP-C3 (Clontech) for the expression of N-terminal GFP-tagged proteins. For C-terminal GFP-tagged hTPC2, the cDNA was placed in pEGFP-N1 (Clontech). For expression of an mCherry-GFP concatemer, the coding sequence of mCherry was inserted in pEGFP-C1 (Clontech). The resulting protein contained a seven-amino acid linker between mCherry and GFP. Constructs for GFP-tagged Rab4, Rab5, Rab7, and Rab11 were kindly provided by Dr. Marino Zerial (Max Planck Institute of Molecular Cell Biology and Genetics, Dresden, Germany), and those for GFP-tagged Lamp1 (Lgp120) and Lamp3 (CD63) were generous gifts from Dr. Paul Luzio (University of Cambridge, Cambridge, United Kingdom).

HEK293 cells were grown in DMEM (high glucose) containing 10% heat-inactivated fetal bovine serum, 100 units/ml penicillin, and 100 $\mu$g/ml streptomycin at 37 °C and 5% $CO_2$. Stable cell lines were made by transfection with the desired cDNA constructs using Lipofectamine 2000 (Invitrogen), followed by selection in the appropriate antibiotics (400 $\mu$g/ml G418 (Invitrogen), 100 $\mu$g/ml Zeocin, or 50 $\mu$g/ml hygromycin B (Roche Diagnostics)). Clonal cell lines were established by limiting dilution as described (16).

*Subcellular Localization Studies*—To view the subcellular locations of the expressed fluorescent protein-tagged proteins, cells were seeded on poly-L-ornithine-coated 15-mm round coverslips and grown overnight. Cells were then washed once with PBS and fixed in 4% paraformaldehyde in PBS at room temperature (~22 °C) for 2 h. After fixation, the coverslip was washed twice with PBS and mounted on glass slides using BioMeda gel mount. Images were taken using a Leica TCS SL laser-scanning confocal system on a Leica DMIRE2 inverted microscope with a 100 × 1.4 numerical aperture oil immersion objective and Leica confocal software (version 2.61). The Pearson correlation coefficient for colocalization between two fluorescent protein-tagged proteins was calculated as described previously (1).

*$Ca^{2+}$ Imaging*—Cells were incubated for 30 min with 5 $\mu$M Fura-2-acetoxymethyl ester in nominally $Ca^{2+}$-free physiological salt solution in an experimental chamber, which was then placed on a Leica DMIRBE inverted microscope after washing with $Ca^{2+}$-containing, Fura-2-free physiological salt solution for at least 30 min prior to experimentation. The physiological salt solution contained 130 mM NaCl, 5.2 mM KCl, 1 mM $MgCl_2$, 1.7 mM $CaCl_2$, 10 mM glucose, and 10 mM Hepes (pH 7.45). The cytoplasmic $Ca^{2+}$ concentration was reported by Fura-2 fluorescence ratio ($F_{340}/F_{380}$ excitation, emission at 510 nm). Emitted fluorescence was recorded at 22 °C with a sampling frequency of 0.5 Hz using a Hamamatsu C4880 CCD camera via a Zeiss Fluar 40×, 1.3 numerical aperture oil immersion objective. Background subtraction was performed on-line. Analysis was carried out using Openlab imaging software (Improvision, Coventry, United Kingdom).

*Intracellular Dialysis*—NAADP (10 nM) was applied intracellularly to single cells in the whole-cell configuration of the patch-clamp technique (voltage-clamp mode, holding potential of −40 mV). The pipette solution contained 140 mM KCl, 10 mM Hepes, 1 mM $MgCl_2$, and 5 $\mu$M Fura-2 (free acid) at pH 7.4, nominally $Ca^{2+}$-free (~100 nM). The seal resistance was ≥3 gigaohms throughout each experiment. The series resistance and pipette resistance were ≤10 megaohms and ≤3 megaohms, respectively, as measured by an Axopatch 200B amplifier (Axon Instruments).

*Co-immunoprecipitation*—N-terminal mCherry-tagged hTPC1, hTPC2, rTPC3, and cTPC3 were transiently transfected individually into the stable HEK293 cell line expressing HA-tagged hTPC2 (1) seeded on 100-mm dishes using Lipofectamine 2000. At 48 h post-transfection, cells were washed with PBS and then homogenized in 0.4 ml of immunoprecipitation buffer containing 150 mM NaCl, 0.5% Triton X-100, and 10 mM Tris (pH 7.5) supplemented with protease inhibitor mixture (Roche Diagnostics) at 4 °C using a sonic dismembrator (Fisher Scientific). Immunoprecipitation was carried out using a rabbit anti-mCherry antibody (1:300; BioVision) and protein A-agarose beads (Millipore), followed by Western blotting using a rat anti-HA monoclonal antibody (1:1000; Roche Diagnostics). For treatment with peptide:*N*-glycosidase F (PNGase F), proteins bound to the protein A beads were treated with 1000 units of PNGase F (New England Biolabs) at room temperature for 30 min before addition of the loading buffer for Western blotting. For Western blotting of mCherry-containing proteins, the anti-mCherry antibody was diluted at 1:1000.

*FRET*—Pairs of GFP- and mCherry-tagged TPCs were cotransfected into HEK293 cells seeded on poly-L-ornithine-coated 15-mm round coverslips and grown for 2 days. Cells were then washed with PBS, fixed in 4% paraformaldehyde, and mounted as described above. FRET signals between GFP (donor) and mCherry (acceptor) were measured using a Leica TCS SP5 (LAS AF) confocal system. Fluorescent signals of the donor, FRET, and acceptor were acquired sequentially line by line. All parameters for the measurements, including gain and

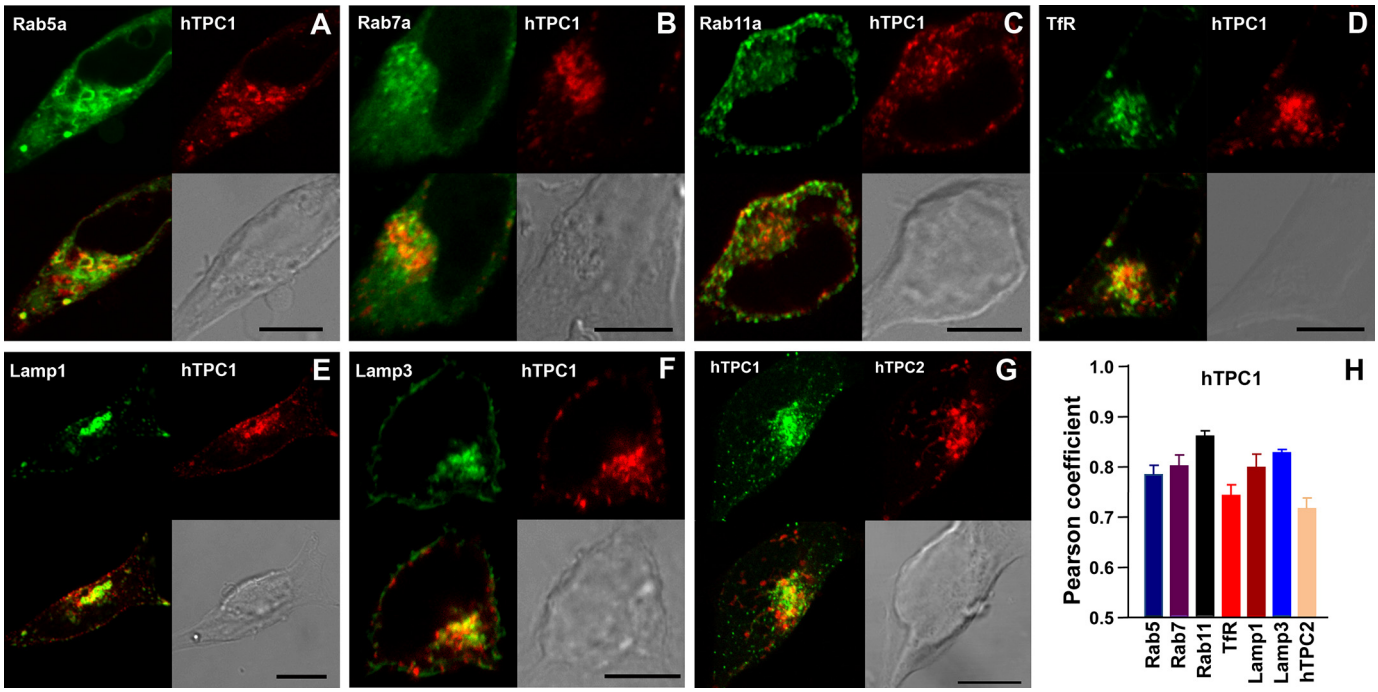


FIGURE 1. **Subcellular localization of hTPC1 stably expressed in HEK293 cells.** *A–F*, stable cell lines were made in HEK293 cells using mCherry-tagged hTPC1 (*red*) and GFP-tagged organelle markers (*green*). The *upper panels* of each image show a GFP-labeled organelle (*left*) and mCherry-labeled hTPC1 (*right*). *G*, a stable HEK293 cell line that expressed GFP-hTPC1 (*green*; *left*) and mCherry-hTPC2 (*red*; *right*). The *lower panels* for all images show a merged image (colocalization in *yellow*; *left*) and a bright-field image for the cell (differential interference contrast; *right*). *Scale bars* = 10 $\mu$m. *H*, Pearson coefficients for cells exemplified in *A–G*. Data are means ± S.E. of three cells for each pair. *TfR*, transferrin receptor.

pinhole settings, excitation intensities, emission detection window, zoom, format, and scan speed, were the same for all samples. Calibration was performed using cells that expressed either GFP- or mCherry-tagged TPC only. FRET efficiency was determined using the default routine by the Leica system with the following formula: $E_A(i) = (B - \beta A - \gamma C)/C$, where A, B, and C represent intensities of donor, FRET, and acceptor, and $\beta$ and $\gamma$ are calibration factors generated by acceptor-only and donor-only references.

*Data Presentation and Statistical Analysis*—Data are presented as means ± S.E. Comparisons between groups were performed using a two-sample *t* test. Probability values $<0.05$ were considered to be statistically significant.

*Drugs and Chemicals*—All compounds were from Sigma-Aldrich unless noted otherwise.

## RESULTS

We first determined the intracellular organelles to which mCherry-tagged hTPC1, hTPC2, cTPC3, and rTPC3 were targeted when stably expressed in HEK293 cells. To minimize interference from nonspecific background staining of antibodies, GFP-tagged organelle markers Rab4, Rab5, Rab7, Rab11, human transferrin receptor, Lamp1, and Lamp3 were coexpressed individually with each of the mCherry-tagged TPCs, and green and red fluorescent signals were analyzed by confocal microscopy. As reported previously (1), hTPC1 partially colocalizes with markers for early (Rab5), late (Rab7), and recycling (Rab11) endosomes (17), as well as for lysosomes (Lamp1 and Lamp3) (Fig. 1). Due to the limitations with respect to the spatial resolution of light microscopy, closely adjacent vesicles separated by <200 nm are not resolvable. As such, a green-labeled vesicle will appear colocalized with a neighboring red-labeled vesicle if the two vesicles are very close to each other, which will be especially common in areas where different endosomal populations and lysosomes are clustered. On the other hand, the fluorescence intensities vary greatly among vesicles; merging of strong green signals with weak red signals, or vice versa, will not necessarily reveal a clear-cut colocalization. As such, Pearson coefficient analyses did not reveal a strong colocalization preference of hTPC1 with any of the organelle markers (Fig. 1*H*). Therefore, these results can be interpreted only as hTPC1 likely being present in a subpopulation of endolysosomes, but the exact nature of this population is not known at present.

On the other hand, mCherry-hTPC2 showed much more complete colocalization with GFP-Lamp1 and GFP-Lamp3 than the other organelle markers (Fig. 2), indicating that hTPC2 is preferentially localized on lysosomal membranes. This result is entirely consistent with our previous immunocytochemical data (1). Of note is that the subcellular distribution of Lamp3 is broader than lysosomes and includes plasma membrane and late endosomes; therefore, some Lamp3-positive regions appeared to be hTPC2-negative (Fig. 2*F*). Nonetheless, these results do not exclude the possibility that in addition to lysosomes, hTPC2 is also present in certain populations of endosomes. However, supporting the idea that TPC1 and TPC2 are expressed in different endolysosomal populations (1), mCherry-hTPC2 and GFP-hTPC1 showed mostly separate distributions (Fig. 1, *G* and *H*).

In contrast to hTPC1 and hTPC2, mCherry-tagged cTPC3 showed nearly complete colocalization with GFP-Rab11 and GFP-human transferrin receptor, but colocalization with GFP-

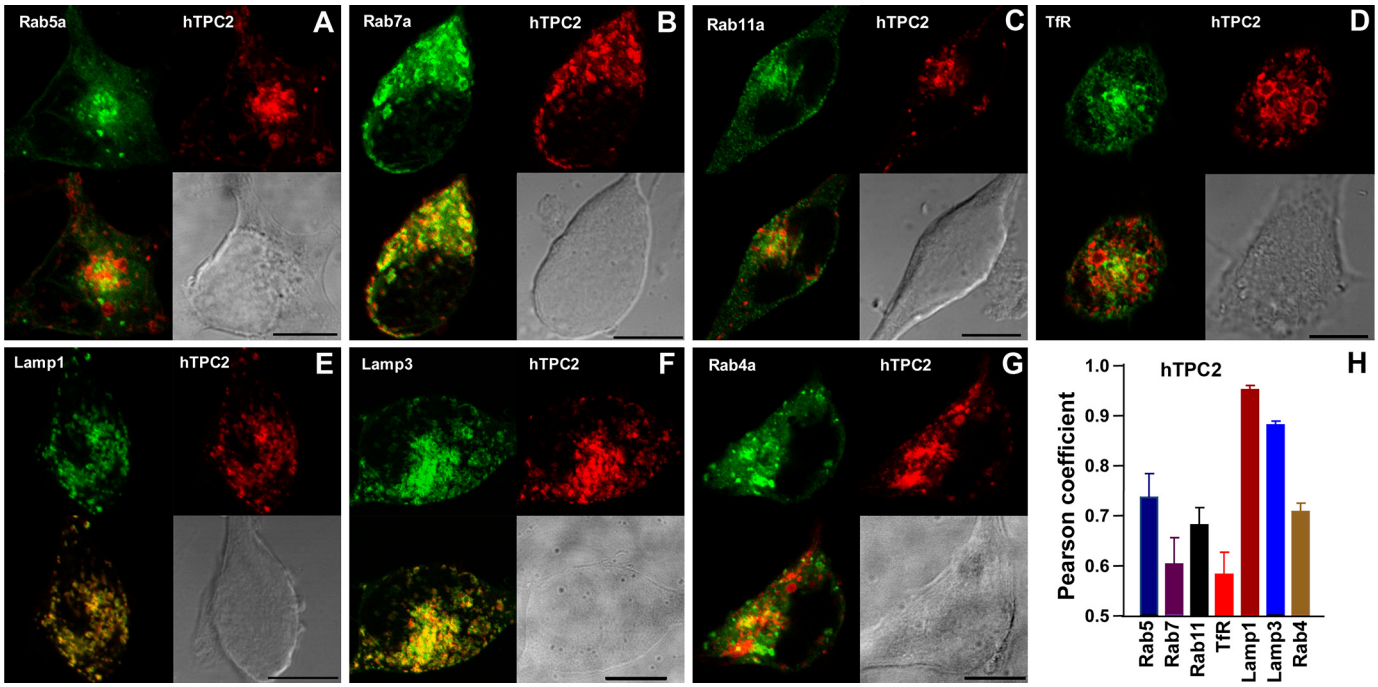


FIGURE 2. **Subcellular localization of hTPC2 stably expressed in HEK293 cells.** *A–G*, stable cell lines were made in HEK293 cells using mCherry-tagged hTPC2 (*red*) and GFP-tagged organelle markers (*green*). The *upper panels* of each image show a GFP-labeled organelle (*left*) and mCherry-labeled hTPC2 (*right*). The *lower panels* show a merged image (colocalization in *yellow*; *left*) and a bright-field image for the cell (*right*). *Scale bars* = 10 $\mu$m. *H*, Pearson coefficients for cells exemplified in *A–G*. Data are means ± S.E. of three cells for each pair. *TfR*, transferrin receptor.

Rab5 (data not shown), Rab7, or Lamp1 was relatively poor (Fig. 3*A*), suggesting a preference for recycling endosomes. However, the distribution of mCherry-tagged rTPC3 was different from that of cTPC3, showing more widespread colocalization with most organelle markers tested, especially Lamp3 (Fig. 3*B*), which is widely distributed among multiple endolysosomal populations. Thus, TPC3 proteins from two different species of vertebrates show different subcellular distribution patterns when stably expressed in HEK293 cells. Given that human cells do not endogenously express TPC3 (1), this difference may arise from aberrant regulation of the subcellular distribution of TPC3 in HEK293 cells.

We next sought to determine whether or not the nature of the $Ca^{2+}$ signals evoked by NAADP varied in a manner dependent on the TPC subtype expressed and their subcellular distribution. NAADP was applied to a variety of HEK293 cell lines by intracellular dialysis from a patch pipette in the whole-cell configuration of the patch-clamp technique and under voltage-clamp conditions (holding potential of −40 mV). Changes in intracellular $Ca^{2+}$ were reported by the fluorescence ratio ($F_{340}/F_{380}$) of the $Ca^{2+}$ indicator Fura-2.

As reported previously (1, 18), intracellular dialysis of 10 nM NAADP failed to evoke a significant $Ca^{2+}$ transient in wild-type HEK293 cells (Fig. 4*A*, *panel i*), which express very low levels of TPC1 and TPC2 and do not express TPC3 (1, 19). However, a marked and transient increase in the Fura-2 fluorescence ratio was triggered by intracellular dialysis of 10 nM NAADP in cells that stably overexpressed mCherry-tagged hTPC1, hTPC2, or rTPC3, but was without effect in either wild-type HEK293 cells or HEK293 cells stably expressing cTPC3. Fig. 4*A* (*panel i*) shows that 10 nM NAADP induced a $Ca^{2+}$ transient in HEK293 cells that stably expressed endosome-targeted hTPC1, as indicated by an increase in the $F_{340}/F_{380}$ ratio from 0.37 ± 0.04 to 0.74 ± 0.07 ($n$ = 17). In contrast, NAADP (10 nM) failed to evoke an identifiable $Ca^{2+}$ transient in wild-type HEK293 cells (*black trace*; $F_{340}/F_{380}$ ratio increasing from 0.41 ± 0.02 to 0.44 ± 0.01, $n$ = 15). Significantly, NAADP evoked only small and spatially restricted $Ca^{2+}$ bursts in hTPC1-expressing cells, which did not propagate across the entire area of the cell. That this was the case is evident from the percentage area of the cell covered by increases in the $F_{340}/F_{380}$ ratio at the peak of the evoked $Ca^{2+}$ transient, which measured 39.24 ± 4.45% ($n$ = 17). In contrast, 10 nM NAADP evoked a larger and global $Ca^{2+}$ transient, which propagated across the entire surface area of all cells that stably expressed lysosome-targeted hTPC2, with the $F_{340}/F_{380}$ ratio increasing from 0.28 ± 0.01 to 1.22 ± 0.06 ($n$ = 23) (Fig. 4*B*, *panel i*). Surprisingly, NAADP evoked an even larger global $Ca^{2+}$ transient in cells that expressed the endolysosome-targeted rTPC3, as indicated by the $F_{340}/F_{380}$ ratio increasing from 0.38 ± 0.04 to 1.59 ± 0.24 ($n$ = 11) (Fig. 4*C*, *panel i*, *black trace*). In contrast to the above, 10 nM NAADP (*red trace*) failed to evoke an increase in the Fura-2 fluorescence ratio in HEK293 cells that expressed cTPC3 ($n$ = 4) (Fig. 4*C*, *panel i*, *blue trace*), which is specifically targeted to recycling endosomes in HEK293 cells. Thus, all the three vertebrate TPC subtypes may support NAADP-induced $Ca^{2+}$ signals, with only lysosome-targeted hTPC2 and rTPC3 able to support global $Ca^{2+}$ transients. However, it appears that the targeting of cTPC3 to a subpopulation of endosomes in this human cell line likely compromises its ability to support $Ca^{2+}$ signals in response to NAADP.

That the nature of the $Ca^{2+}$ signal evoked via hTPC1 may differ from that evoked via either hTPC2 or rTPC3 was confirmed by pharmacological interventions. Fig. 4 (*A–C*, *panel ii*)

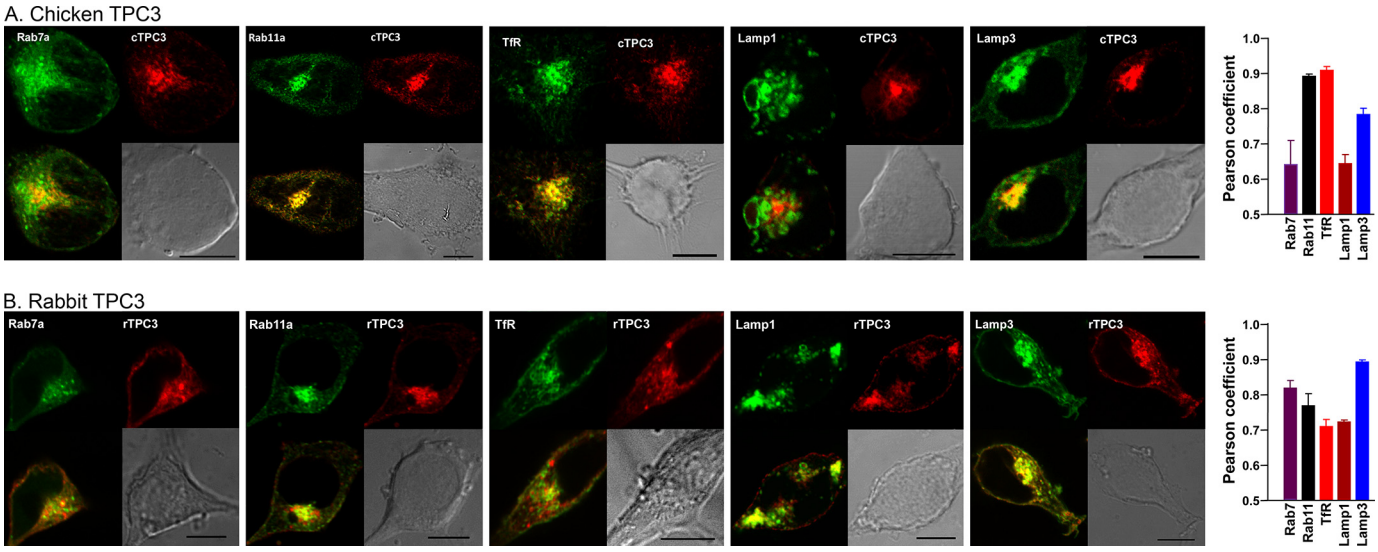


FIGURE 3. **Different subcellular localizations of cTPC3 and rTPC3 when stably expressed in HEK293 cells.** Stable cell lines were made in HEK293 cells using mCherry-tagged (*red*) cTPC3 (*A*) or rTPC3 (*B*) and GFP-tagged organelle markers (*green*). The *upper panels* of each image show a GFP-labeled organelle (*left*) and mCherry-labeled TPC3 (*right*). The *lower panels* show a merged image (colocalization in *yellow*; *left*) and a bright-field image (*right*). *Scale bars* = 10 $\mu$m. Pearson coefficients for cells exemplified in the images are shown on the right. Data are means ± S.E. of three cells for each pair. *TfR*, transferrin receptor.

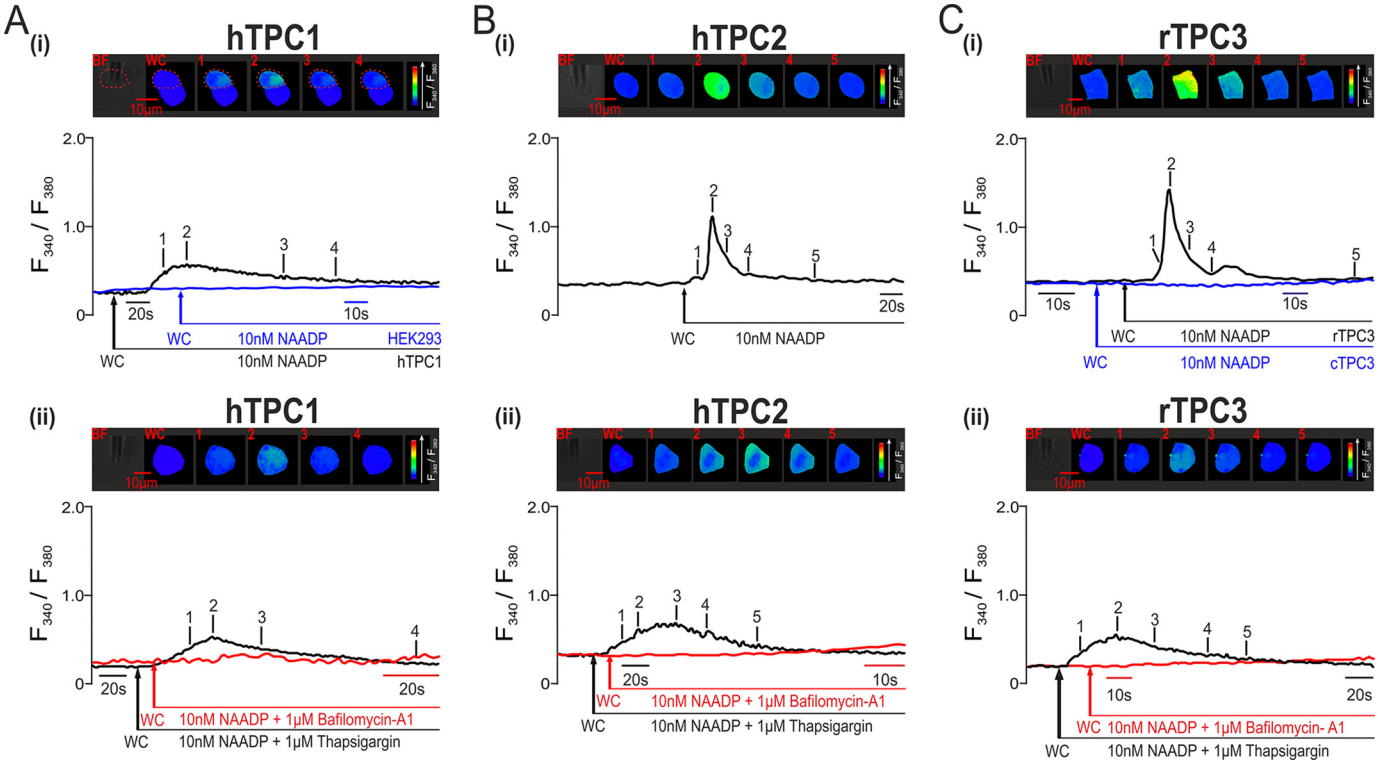


FIGURE 4. **NAADP-dependent $Ca^{2+}$ signals via TPC2 and TPC3 (but not TPC1) couple to ER $Ca^{2+}$ release in HEK293 cells.** In *A* (*panel i*), the *upper panel* shows a bright-field image of a HEK293 cell that stably overexpressed hTPC1 and a series of pseudo-color images of the Fura-2 fluorescence ratio ($F_{340}/F_{380}$) recorded in the same cell (indicated by *dashed red lines*) during intracellular dialysis from a patch pipette of 10 nM NAADP. The *lower panel* shows the corresponding record of the $F_{340}/F_{380}$ ratio against time upon intracellular dialysis of 10 nM NAADP (*black trace*). The *blue trace* is a record of the $F_{340}/F_{380}$ ratio against time recorded in a wild-type HEK293 cell that was dialyzed with 10 nM NAADP. *WC* indicates the point at which intracellular dialysis commenced on entering the whole-cell configuration. In *panel i* in *B* and *C*, the conditions were similar to those described for *panel i* in *A*, but the HEK293 cells stably expressed hTPC2 (*B*), rTPC3 (*C*, images and *black trace*), or cTPC3 (*C*, *blue trace*), and 10 nM NAADP was introduced by pipette dialysis. In *panel ii* in *A–C*, the conditions were similar to those described for *panel i* in *A–C*, but the cells were preincubated with thapsigargin (1 $\mu$M; images and *black traces*) or bafilomycin $A_1$ (1 $\mu$M; *red traces*) to deplete $Ca^{2+}$ from ER or acidic stores, respectively.

shows that in cells expressing hTPC1, hTPC2, or rTPC3, the $Ca^{2+}$ transient induced by NAADP was abolished by preincubation (≥50 min) with bafilomycin $A_1$ (1 $\mu$M), thus confirming that hTPC1, hTPC2, and rTPC3 do indeed mediate $Ca^{2+}$ release from acidic stores. Intriguingly, however, depletion of ER stores by preincubation (≥40 min) of cells with thapsigargin (1 $\mu$M) had quite different effects on $Ca^{2+}$ signaling via hTPC1 compared with hTPC2 and rTPC3. Fig. 4*A* (*panel ii*) shows that

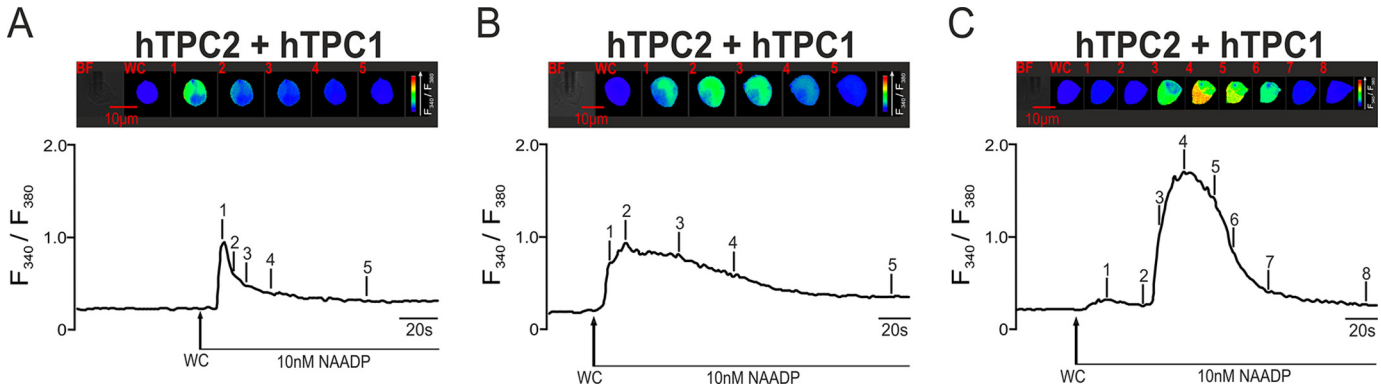


FIGURE 5. **NAADP evokes robust $Ca^{2+}$ transients of variable magnitude in HEK293 cells that stably coexpressed hTPC2 and hTPC1.** In *A*, the *upper panel* shows a bright-field image of a HEK293 cell that stably overexpressed hTPC2 and hTPC1 and a series of pseudo-color images of the Fura-2 fluorescence ratio ($F_{340}/F_{380}$) recorded in the same cell during intracellular dialysis from a patch pipette of 10 nM NAADP. The *lower panel* shows the corresponding record of the $F_{340}/F_{380}$ ratio against time. *B* and *C* show two additional examples of the $Ca^{2+}$ transients of varied magnitude evoked by NAADP in cells that coexpressed hTPC1 and hTPC2. *WC* indicates the point at which intracellular dialysis commenced on entering the whole-cell configuration.

thapsigargin was without effect on the $Ca^{2+}$ transient evoked by 10 nM NAADP in cells that stably overexpressed hTPC1, with the $F_{340}/F_{380}$ ratio increasing from 0.30 ± 0.03 to 0.58 ± 0.06 ($n$ = 8). In contrast, thapsigargin markedly attenuated $Ca^{2+}$ signals in cells expressing lysosome-targeted hTPC2 (Fig. 4*B*, *panel ii*), with the $F_{340}/F_{380}$ ratio increasing from 0.28 ± 0.01 to 1.22 ± 0.06 ($n$ = 23) in the absence of thapsigargin and from 0.25 ± 0.01 to 0.58 ± 0.03 ($n$ = 9) in its presence. A similar attenuation of the $Ca^{2+}$ transient was also observed with respect to endolysosome-targeted rTPC3 (Fig. 4*C*, *panel ii*), with the $F_{340}/F_{380}$ ratio increasing from 0.38 ± 0.04 to 1.81 ± 0.28 ($n$ = 8) in the absence of thapsigargin and from 0.26 ± 0.02 to 0.58 ± 0.09 ($n$ = 5) in its presence. Given that the absolute magnitude of the transient evoked by NAADP via hTPC1, hTPC2, and rTPC3 was not significantly different after depletion of ER $Ca^{2+}$ stores by thapsigargin, these data provide the strongest possible support for the view that hTPC1 and therefore endosomes are unable to support $Ca^{2+}$ signals that couple by $Ca^{2+}$-induced $Ca^{2+}$ release (CICR) to ER stores. In contrast, it is clear that lysosome-targeted hTPC2 and endolysosome-targeted rTPC3 are able to couple to the ER.

The fact that rTPC3 is able to support $Ca^{2+}$ signals when expressed in HEK293 cells brings into question the proposal that TPC3 may function as a dominant-negative subtype. To examine this possibility further, we studied the nature of NAADP-dependent $Ca^{2+}$ signaling in HEK293 cells that stably coexpressed hTPC2 and hTPC1, hTPC2 and cTPC3, and hTPC2 and rTPC3. Fig. 5 shows three different example records of the $Ca^{2+}$ transient evoked by 10 nM NAADP in cells that coexpressed hTPC1 and hTPC2; on average, the $F_{340}/F_{380}$ ratio increased from 0.27 ± 0.02 to 1.02 ± 0.11 ($n$ = 9). Clearly, the magnitude and time course of the response varied markedly between cells, suggesting that under the conditions of our experiments, there is a degree of plasticity with respect to the organization of endolysosomal stores in cells that coexpress hTPC1 and hTPC2. In contrast, the transient evoked by NAADP in cells that coexpressed hTPC2 and cTPC3 was slightly smaller in magnitude, with the $F_{340}/F_{380}$ ratio increasing from 0.28 ± 0.01 to 0.82 ± 0.07 ($n$ = 5) (Fig. 6*A*). However, in each case, a global $Ca^{2+}$ transient was evoked. Given this and our previous observations with respect to rTPC3, it was all the more surprising to find that NAADP (10 nM or 1 μM) failed to evoke a $Ca^{2+}$ transient in cells that coexpressed hTPC2 and rTPC3; the $F_{340}/F_{380}$ ratio remained relatively stable at 0.37 ± 0.02 after entering the whole-cell configuration and at 0.39 ± 0.02 after 120 s ($n$ = 7) (Fig. 6*B*). This was particularly so given that 1 μM bafilomycin $A_1$ evoked a robust $Ca^{2+}$ transient in these cells, with the $F_{340}/F_{380}$ ratio increasing from 0.25 ± 0.01 to 0.64 ± 0.04 ($n$ = 13) (Fig. 6*C*). The lack of response to NAADP therefore did not result from a high constitutive TPC activity and consequent depletion of acidic stores. That rTPC3 functions to support NAADP-dependent $Ca^{2+}$ signals when expressed alone argues against it being a true dominant-negative TPC subtype, although there is clearly some form of a negative interaction between rTPC3 and hTPC2 when coexpressed. All $Ca^{2+}$ imaging results are summarized in Fig. 7.

To further probe the relationship between TPC2 and other TPC isoforms, we performed co-immunoprecipitation (co-IP) experiments using HEK293 cells that coexpressed HA-hTPC2 (4) and mCherry-tagged hTPC1, hTPC2, rTPC3, or cTPC3 (all N-terminally tagged). After immunoprecipitation of cell lysates by an anti-mCherry antibody, the presence of HA-hTPC2 in the precipitated complexes was examined by Western blotting using an anti-HA antibody. Because of glycosylation and the presence of some TPC dimers, multiple bands were detected for HA-hTPC2, with dominant bands found at ~85 kDa and a weaker band slightly above 150 kDa (Fig. 8*A*). Bands of similar sizes were detected in immunoprecipitated samples obtained from cells that coexpressed HA-hTPC2 with any of the mCherry-TPCs, but not that with the mCherry vector (Fig. 8*B*, *left panel*). The band intensities were higher with mCherry-hTPC2 than with other mCherry-TPCs, but there was no obvious difference among hTPC1, rTPC3, and cTPC3. Strikingly, although the ~85-kDa band in the mCherry-hTPC2 pulldown sample was reduced in size by treatment with PNGase F, indicating glycosylation of HA-hTPC2, those in the mCherry-hTPC1, rTPC3, and cTPC3 pulldown samples were largely unaffected (Fig. 8*B*, *right panel*). On the other hand, PNGase F treatment reduced the ~150-kDa bands in all samples. These results suggest different post-translational modifications on TPC2 when it is associated with TPC1 or TPC3, which could indicate differential compartmentalization or subcellular struc-

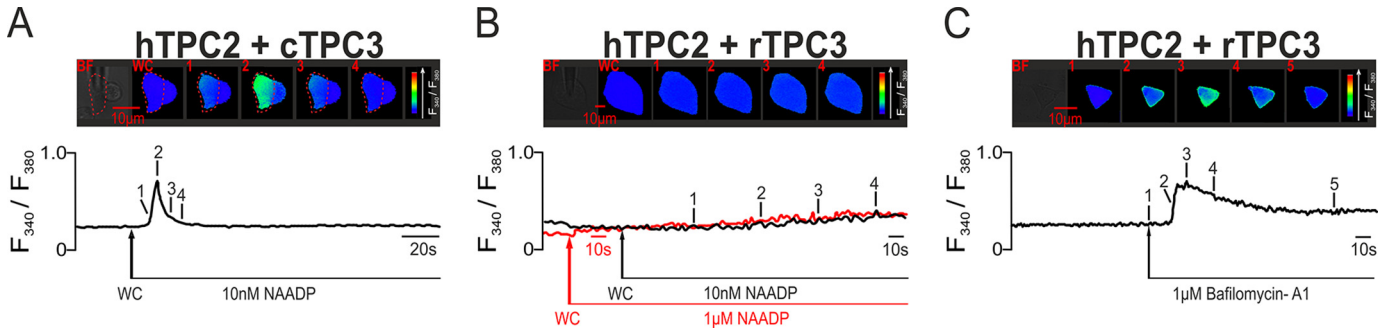


FIGURE 6. **NAADP evokes robust $Ca^{2+}$ signals in HEK293 cells that stably coexpressed hTPC2 and cTPC3, but failed to evoke any such response in cells that coexpressed hTPC2 and rTPC3.** In *A*, the *upper panel* shows a bright-field image of a HEK293 cell that stably overexpressed hTPC2 and cTPC3 and a series of pseudo-color images of the Fura-2 fluorescence ratio ($F_{340}/F_{380}$) recorded in the same cell during intracellular dialysis from a patch pipette of 10 nM NAADP. The *lower panel* shows the corresponding record of the $F_{340}/F_{380}$ ratio against time. In *B*, the *upper panel* shows a bright-field image of a HEK293 cell that stably overexpressed hTPC2 and rTPC3 and a series of pseudo-color images of the Fura-2 fluorescence ratio ($F_{340}/F_{380}$) recorded in the same cell during intracellular dialysis from a patch pipette of 10 nM NAADP. The *lower panel* shows the corresponding record of the $F_{340}/F_{380}$ ratio against time (*black trace*). The *red trace* shows the $F_{340}/F_{380}$ ratio against time for a different cell that stably overexpressed hTPC2 and rTPC3 during intracellular dialysis from a patch pipette of 1 μM NAADP. In *C*, the *upper panel* shows a bright-field image of a HEK293 cell that stably overexpressed hTPC2 and rTPC3 and a series of pseudo-color images of the $F_{340}/F_{380}$ ratio recorded in the same cell during extracellular application of 1 μM bafilomycin $A_1$. The *lower panel* shows the corresponding record of the $F_{340}/F_{380}$ ratio against time. *WC* indicates the point at which intracellular dialysis commenced on entering the whole-cell configuration.

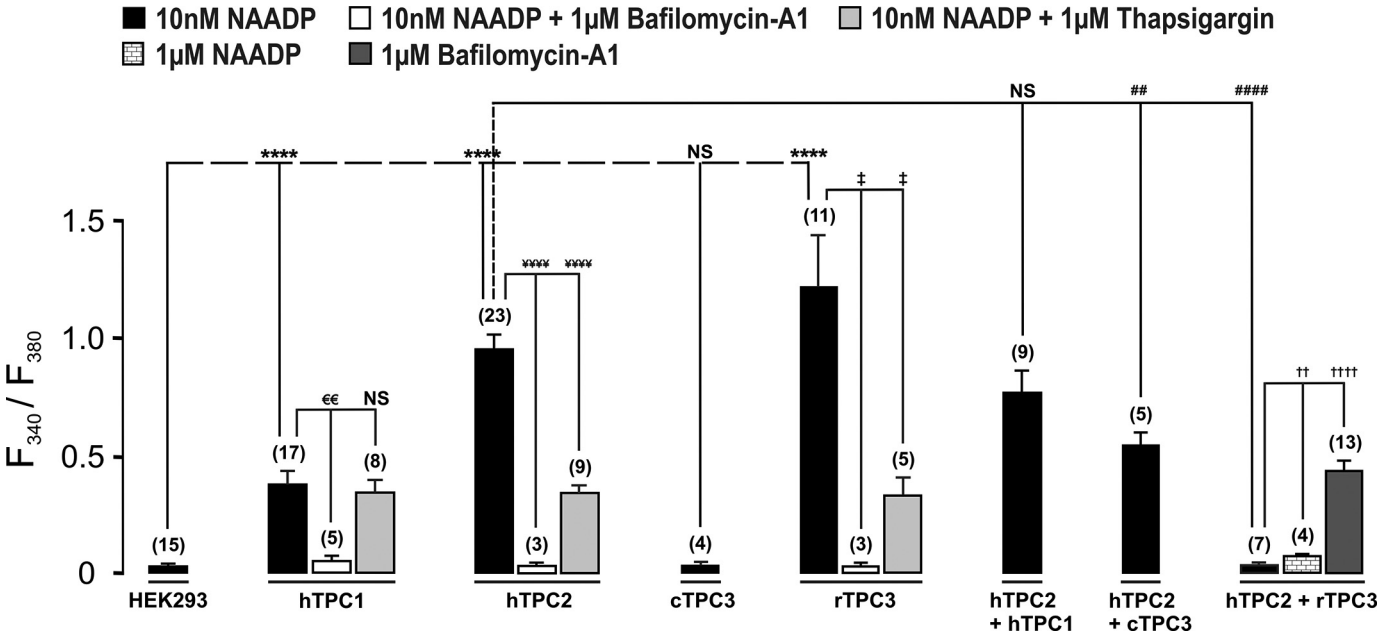


FIGURE 7. **Comparison of the peak change in $F_{340}/F_{380}$ ratio induced by NAADP in HEK293 cells that stably expressed TPC1, TPC2, and/or TPC3.** The bar chart shows means ± S.E. for the peak change in Fura-2 fluorescence ratio induced by NAADP in HEK293 cells that stably expressed TPC1, TPC2, and/or TPC3 under all experimental conditions as indicated. Data are means ± S.E. for the number of cells indicated in *parentheses*. ‡, $p < 0.05$; €€, ##, and ††, $p < 0.01$; ****, ¥¥¥¥, ####, and ††††, $p < 0.0001$ determined by two-sample *t* test between the *identified bar* and the *leftmost bar* within group compared. *NS*, not significant.

tures for hTPC2 and its partners. However, despite the more prominent presence of rTPC3 in lysosomes compared with hTPC1 and cTPC3, it did not pull down more TPC2 than the other two TPC isoforms, and the HA-TPC2 associated with rTPC3 was equally resistant to deglycosylation by PNGase F as it was when associated with the other two TPC isoforms. Therefore, these experiments were uninformative about any specific interaction between hTPC2 and rTPC3 that might explain the loss of NAADP-evoked $Ca^{2+}$ response in cells that coexpressed these two proteins.

Next, we studied possible interactions between hTPC2 and other TPC isoforms using FRET. HEK293 cells were coexpressed with GFP-tagged hTPC2 and N-terminal mCherry-tagged hTPC1, rTPC3, and cTPC3. Because homodimer formation is obligatory in cells expressing only hTPC2, mCherry-hTPC2 was coexpressed with GFP-tagged hTPC2 as a positive control. The GFP tag was added to either the N or C terminus of hTPC2 to reveal any orientation effect on the dimer (or complex) formation. To minimize the interference on the sequentially acquired fluorescent signals by the rapidly moving endolysosomal vesicles (1), FRET was measured using fixed cells. Interestingly and unexpectedly, the FRET efficiency was significantly higher when both fluorescent protein tags were at the N terminus of hTPC2 than when GFP was added to the C terminus of one construct and mCherry was added to the N terminus of another construct (Fig. 8*C*), indicating a head-to-head assembly of the dimeric channel. Even more surprising and unexpected from the co-IP experiments, the FRET efficiency between GFP-hTPC2 and mCherry-hTPC1 was similar to, if not higher than, that between GFP-hTPC2 and mCherry-

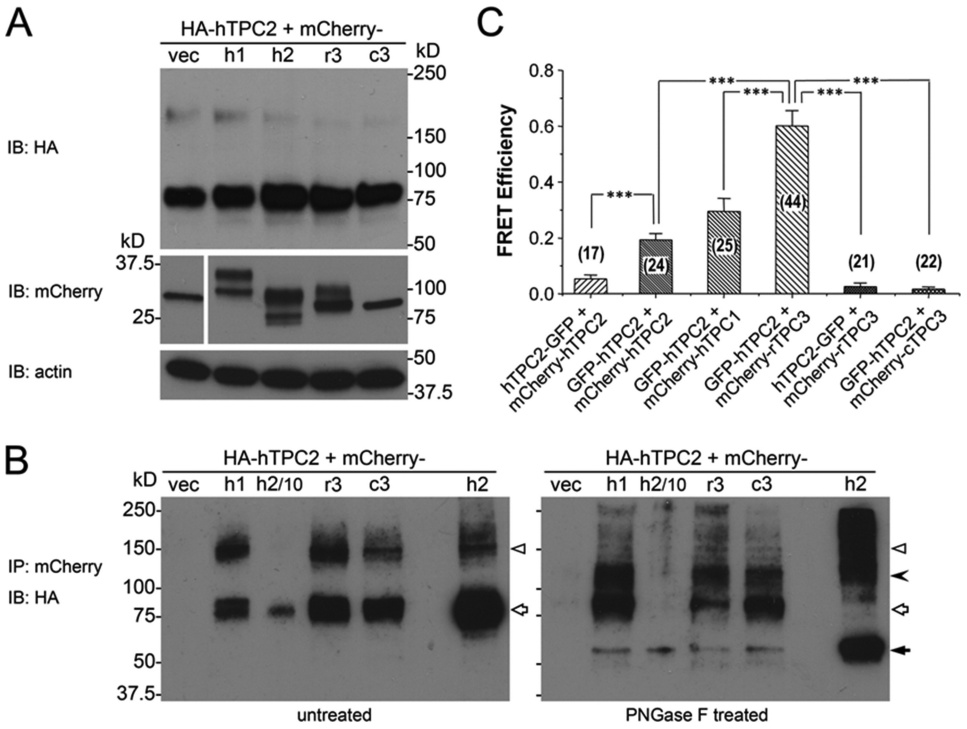


FIGURE 8. **Interaction between hTPC2 and other TPC isoforms when coexpressed in HEK293 cells.** *A*, expression levels detected by immunoblotting (*IB*) of HA-hTPC2 (*upper panel*), mCherry (*middle left panel*), and mCherry-tagged TPC isoforms (*middle right panel*) in stable HA-hTPC2 cells transiently transfected with the cDNA for mCherry (*vec*) and N-terminal mCherry-tagged hTPC1 (*h1*), hTPC2 (*h2*), rTPC3 (*r3*), or cTPC3 (*c3*). Actin was used as a loading control (*lower panel*). *B*, co-IP of HA-hTPC2 by the anti-mCherry antibody. The immunoprecipitants were left untreated (*left panel*) or treated with PNGase F (*right panel*). Samples from mCherry-hTPC2-transfected cells (*h2*) were loaded as 1/10 (*h2/10*) and equivalent (h2) amounts compared with the other samples for immunoblotting. *Open triangles* indicate possible dimers. The *filled arrowhead* indicates reduced size of possible dimers after deglycosylation by PNGase F. *Open arrows* indicate the ~85-kDa band mostly unaffected by PNGase F except for the mCherry-hTPC2-transfected cell samples. The *filled arrow* indicates the reduced size from the ~85-kDa band. *C*, FRET efficiency between GFP and mCherry in HEK293 cells that coexpressed GFP-tagged hTPC2 (either N- or C-terminal tag) and N-terminal mCherry-tagged TPC isoforms as indicated. Data are means ± S.E. for the number of cells indicated in *parentheses*. ***, $p < 0.001$ determined by two-sample *t* test between the indicated groups.

hTPC2. Notably, however, the FRET efficiency between GFP-hTPC2 and mCherry-rTPC3 was the highest among all tested pairs (Fig. 8*C*). The FRET efficiency between GFP-hTPC2 and mCherry-rTPC3 (0.60 ± 0.05, $n = 44$) approached that achieved by an mCherry-GFP concatemer (0.66 ± 0.02, $n = 20$) under the same experimental conditions, indicating very close interactions between hTPC2 and rTPC3, at least in fixed cells. Again, the high FRET efficiency was detected only with the tags added to the N termini. The FRET efficiency between C-terminal GFP-tagged hTPC2 (hTPC2-GFP) and N-terminal mCherry-tagged rTPC3 (mCherry-rTPC3) was 0.026 ± 0.013 ($n = 21$), which is not different from that of the negative control (0.035 ± 0.016, $n = 14$) measured in cells that coexpressed GFP and mCherry encoded by two separate expression constructs. Consistent with the $Ca^{2+}$ imaging data that cTPC3 failed to affect hTPC2-mediated NAADP responses, the FRET efficiency of GFP-hTPC2 and mCherry-cTPC3 (0.016 ± 0.009, $n = 22$) was similar to that of the negative control. Therefore, the FRET experiments indeed suggest a peculiar interaction between hTPC2 and rTPC3, which may explain the selective loss of NAADP-evoked $Ca^{2+}$ transients in cells that coexpressed these two proteins.

## DISCUSSION

In this study, we have shown that when stably expressed in HEK293 cells, hTPC1 and cTPC3 were restricted primarily to different subpopulations of endosomes. In contrast, hTPC2 was specifically targeted to lysosomes, whereas rTPC3 was more widely distributed across both endosomes and lysosomes. Given these findings, we were able to assess the capacity of vertebrate TPC3 to support $Ca^{2+}$ signaling in response to NAADP and also the capacity of endosomes and lysosomes to couple to the ER by CICR.

All three subtypes of vertebrate TPC supported $Ca^{2+}$ release from acidic stores. This was evident from the fact that their expression in HEK293 cells markedly enhanced the ability of NAADP to elicit $Ca^{2+}$ signals. Consistent with this view, stable expression of hTPC1, hTPC2, and rTPC3, but not cTPC3, supported NAADP-evoked $Ca^{2+}$ signals that were blocked by prior depletion of acidic stores with bafilomycin $A_1$. In fact, $Ca^{2+}$ transients evoked by NAADP in cells that stably expressed rTPC3 were of greater magnitude than those observed in cells that overexpressed either hTPC1 or hTPC2. Therefore, rTPC3 is functional when expressed in HEK293 cells, and this provides the strongest possible evidence against the view that vertebrate TPC3 might act as a dominant-negative subtype, as has previously been proposed for sea urchin TPC3 (4). However, our data do suggest that HEK293 cells may be unable to appropriately process all TPCs derived from other species. This is evident from the fact that when stably expressed, cTPC3 is targeted to a subpopulation of endosomes and in a manner that

does not appear to support $Ca^{2+}$ signaling by NAADP. That this may be the case is supported by recent studies on zebrafish TPC3, which is targeted to the plasma membrane when expressed in *Xenopus* oocytes, HEK293T cells, and cultured mouse hippocampal neurons and forms fully functional, non-inactivating, high voltage-activated sodium channels (15). On the other hand, our demonstration that lysosome-targeted rTPC3, despite its widespread expression in other subcellular compartments, can support $Ca^{2+}$ signaling from acidic stores argues strongly in favor of a role for TPC3 in this process when it is appropriately targeted.

The fact that NAADP-dependent $Ca^{2+}$ signaling is enhanced by the expression of hTPC1, hTPC2, and rTPC3, respectively, provides further support for the view that TPCs are of fundamental importance to this process (11), irrespective of the controversy surrounding their ability to conduct $Ca^{2+}$ (9, 10, 13). That hTPC1 was entirely restricted to different subpopulations of endosomes, hTPC2 to lysosomes, and rTPC3 to both endosomes and lysosomes provided us with the opportunity to further assess the capacity for organellar coupling to the ER by CICR. Previously, we have shown that depletion of ER stores by thapsigargin markedly attenuated $Ca^{2+}$ transients induced by NAADP in HEK293 cells that stably overexpressed lysosome-targeted hTPC2 (1). Here, we showed that thapsigargin likewise attenuated $Ca^{2+}$ transients evoked by NAADP in cells that stably expressed endolysosome-targeted rTPC3. In contrast, thapsigargin was entirely without effect on $Ca^{2+}$ transients evoked by NAADP in cells that stably expressed endosome-targeted hTPC1. It therefore seems reasonable to conclude that the capacity for ER coupling is conferred not by a specific TPC, but by the ability of lysosome-targeted TPCs to support $Ca^{2+}$ release from these organelles, at least in HEK293 cells. In this respect, our findings in relation to hTPC1 are entirely inconsistent with previous proposals that hTPC1 and sea urchin TPC1 couple to the ER by CICR when transiently overexpressed in HEK293 cells or SKBR3 cells (4, 6). The only obvious explanation for these contrary data is that transient expression of TPC1, from whatever species, in a human cell line provides for erroneous targeting of TPC1 to lysosomes, which would appear to be supported by the associated colocalization data.

Guided by the unique signature of the NAADP-dependent $Ca^{2+}$ transients conferred by the stable expression of hTPC1, hTPC2, and rTPC3, we next assessed the ability for organelle-specific subunit interactions by stable coexpression of different TPC subunit combinations. We found no evidence of functional deficits with respect to NAADP-dependent $Ca^{2+}$ signals upon co-overexpression of hTPC2 and hTPC1; NAADP-dependent $Ca^{2+}$ signaling was enhanced. Moreover, the view that vertebrate TPC3 is not a dominant-negative subtype gained further support from the finding that coexpression of hTPC2 with the "silent" cTPC3 permitted $Ca^{2+}$ transients that were indistinguishable from those generated in HEK293 cells that overexpressed hTPC1 and hTPC2, although the magnitude of the response was slightly reduced relative to cells that expressed hTPC2 alone.

In marked contrast, however, coexpression of the "fully functional" rTPC3 and hTPC2 ablated NAADP-dependent $Ca^{2+}$ signaling even though $Ca^{2+}$ signals could still be evoked upon depletion of lysosomal stores by bafilomycin $A_1$. This latter finding suggests a negative interaction between two functional TPC subtypes. We therefore assessed the possibility that two different TPC subunits could indeed interact by co-IP and FRET. Even though we found no evidence that rTPC3 associated with hTPC2 any better than hTPC1 or cTPC3 in the co-IP experiments, we detected excellent FRET efficiency between hTPC2 and rTPC3, suggesting very close apposition of these two proteins. However, given the poor level of co-IP, the interaction between hTPC2 and rTPC3 might be rather weak and easily disrupted by the relatively mild detergent condition (0.5% Triton X-100) used in the co-IP experiment. The preferred head-to-head, rather than head-to-tail, interaction could also indicate clustering via N termini, without necessarily involving dimer formation. Indeed, the FRET results do not exclude the possibility that interactions occurred between channels on two separate endolysosomal vesicles juxtaposed against each other because the closely associated vesicles are not resolvable by light microscopy. It is tempting to speculate that such interactions between TPC2 and TPC3, when coexpressed in native cells, might help coordinate organellar interaction and/or membrane fusion events by providing appropriately "timed" modulation of channel gating. However, for now, the precise mechanism and function of the negative impact of interactions between hTPC2 and rTPC3 remain interesting questions that warrant further investigation.

In summary, this study demonstrates that NAADP may trigger intracellular $Ca^{2+}$ release from acidic stores in a manner that can be supported by all three subtypes of vertebrate TPCs, specifically hTPC1, hTPC2, and rTPC3. Therefore, TPC3 does not act as a dominant-negative subtype in vertebrates. Moreover, we have demonstrated that endosome-restricted hTPC1 was unable to confer $Ca^{2+}$ signals of either the necessary magnitude or locale to permit ER coupling by CICR. In contrast, in cells expressing either lysosomal hTPC2 or endolysosomal rTPC3, NAADP was able to trigger a propagating, global $Ca^{2+}$ transient due to subsequent amplification of $Ca^{2+}$ signals from acidic stores by CICR from the ER. Therefore, ER coupling is likely determined by the organelles to which each TPC subtype is targeted and by other organelle-specific moieties. Surprisingly, our study also revealed a physical and functional interaction between hTPC2 and rTPC3, which renders each channel unable to support NAADP-dependent $Ca^{2+}$ release from acidic organelles. The nature of this interaction and the mechanism by which it interferes with channel function are curious and warrant further investigation. Nonetheless, this investigation provides strong support for the view that different cellular processes may be regulated by TPC1 and TPC2 in humans and by TPC3 when expressed in other species.

*Acknowledgments—We thank Drs. Marino Zerial and Paul Luzio for plasmid constructs of GFP-tagged organelle markers.*

## REFERENCES

1. Calcraft, P. J., Ruas, M., Pan, Z., Cheng, X., Arredouani, A., Hao, X., Tang, J., Rietdorf, K., Teboul, L., Chuang, K. T., Lin, P., Xiao, R., Wang, C., Zhu, Y., Lin, Y., Wyatt, C. N., Parrington, J., Ma, J., Evans, A. M., Galione, A., and

Zhu, M. X. (2009) NAADP mobilizes calcium from acidic organelles through two-pore channels. *Nature* **459,** 596–600
2. Ishibashi, K., Suzuki, M., and Imai, M. (2000) Molecular cloning of a novel form (two-repeat) protein related to voltage-gated sodium and calcium channels. *Biochem. Biophys. Res. Commun.* **270,** 370–376
3. Zhu, M. X., Ma, J., Parrington, J., Calcraft, P. J., Galione, A., and Evans, A. M. (2010) Calcium signaling via two-pore channels: local or global, that is the question. *Am. J. Physiol. Cell Physiol.* **298,** C430–C441
4. Ruas, M., Rietdorf, K., Arredouani, A., Davis, L. C., Lloyd-Evans, E., Koegel, H., Funnell, T. M., Morgan, A. J., Ward, J. A., Watanabe, K., Cheng, X., Churchill, G. C., Zhu, M. X., Platt, F. M., Wessel, G. M., Parrington, J., and Galione, A. (2010) Purified TPC isoforms form NAADP receptors with distinct roles for $Ca^{2+}$ signaling and endolysosomal trafficking. *Curr. Biol.* **20,** 703–709
5. Zong, X., Schieder, M., Cuny, H., Fenske, S., Gruner, C., Rötzer, K., Griesbeck, O., Harz, H., Biel, M., and Wahl-Schott, C. (2009) The two-pore channel TPCN2 mediates NAADP-dependent $Ca^{2+}$-release from lysosomal stores. *Pflugers Arch.* **458,** 891–899
6. Brailoiu, E., Churamani, D., Cai, X., Schrlau, M. G., Brailoiu, G. C., Gao, X., Hooper, R., Boulware, M. J., Dun, N. J., Marchant, J. S., and Patel, S. (2009) Essential requirement for two-pore channel 1 in NAADP-mediated calcium signaling. *J. Cell Biol.* **186,** 201–209
7. Cai, X., and Patel, S. (2010) Degeneration of an intracellular ion channel in the primate lineage by relaxation of selective constraints. *Mol. Biol. Evol.* **27,** 2352–2359
8. Brailoiu, E., Hooper, R., Cai, X., Brailoiu, G. C., Keebler, M. V., Dun, N. J., Marchant, J. S., and Patel, S. (2010) An ancestral deuterostome family of two-pore channels mediates nicotinic acid adenine dinucleotide phosphate-dependent calcium release from acidic organelles. *J. Biol. Chem.* **285,** 2897–2901
9. Schieder, M., Rötzer, K., Brüggemann, A., Biel, M., and Wahl-Schott, C. A. (2010) Characterization of two-pore channel 2 (TPCN2)-mediated $Ca^{2+}$ currents in isolated lysosomes. *J. Biol. Chem.* **285,** 21219–21222
10. Wang, X., Zhang, X., Dong, X. P., Samie, M., Li, X., Cheng, X., Goschka, A., Shen, D., Zhou, Y., Harlow, J., Zhu, M. X., Clapham, D. E., Ren, D., and Xu, H. (2012) TPC proteins are phosphoinositide-activated sodium-selective ion channels in endosomes and lysosomes. *Cell* **151,** 372–383
11. Morgan, A. J., and Galione, A. (2014) Two-pore channels (TPCs): current controversies. *BioEssays* **36,** 173–183
12. Jha, A., Ahuja, M., Patel, S., Brailoiu, E., and Muallem, S. (2014) Convergent regulation of the lysosomal two-pore channel-2 by $Mg^{2+}$, NAADP, PI(3,5)P2 and multiple protein kinases. *EMBO J.* **33,** 501–511
13. Pitt, S. J., Funnell, T. M., Sitsapesan, M., Venturi, E., Rietdorf, K., Ruas, M., Ganesan, A., Gosain, R., Churchill, G. C., Zhu, M. X., Parrington, J., Galione, A., and Sitsapesan, R. (2010) TPC2 is a novel NAADP-sensitive $Ca^{2+}$ release channel, operating as a dual sensor of luminal pH and $Ca^{2+}$. *J. Biol. Chem.* **285,** 35039–35046
14. Zhu, M. X., Ma, J., Parrington, J., Galione, A., and Evans, A. M. (2010) TPCs: endolysosomal channels for $Ca^{2+}$ mobilization from acidic organelles triggered by NAADP. *FEBS Lett.* **584,** 1966–1974
15. Cang, C., Aranda, K., and Ren, D. (2014) A non-inactivating high-voltage-activated two-pore $Na^{+}$ channel that supports ultra-long action potentials and membrane bistability. *Nat. Commun.* **5,** 5015
16. Miller, W. R., and Larionov, A. (2011) Molecular effects of oestrogen deprivation in breast cancer. *Mol. Cell. Endocrinol.* **340,** 127–136
17. Sherer, N. M., Lehmann, M. J., Jimenez-Soto, L. F., Ingmundson, A., Horner, S. M., Cicchetti, G., Allen, P. G., Pypaert, M., Cunningham, J. M., and Mothes, W. (2003) Visualization of retroviral replication in living cells reveals budding into multivesicular bodies. *Traffic* **4,** 785–801
18. Ogunbayo, O. A., Zhu, Y., Rossi, D., Sorrentino, V., Ma, J., Zhu, M. X., and Evans, A. M. (2011) Cyclic adenosine diphosphate ribose activates ryanodine receptors, whereas NAADP activates two-pore domain channels. *J. Biol. Chem.* **286,** 9136–9140
19. Aoyama, M., Yamada, A., Wang, J., Ohya, S., Furuzono, S., Goto, T., Hotta, S., Ito, Y., Matsubara, T., Shimokata, K., Chen, S. R., Imaizumi, Y., and Nakayama, S. (2004) Requirement of ryanodine receptors for pacemaker $Ca^{2+}$ activity in ICC and HEK293 cells. *J. Cell Sci.* **117,** 2813–2825